Accepted Manuscript

Influence of surface energetics of graphene oxide on fracture toughness of epoxy nanocomposites

Woo-Seok Kang, Kyong Yop Rhee, Soo-Jin Park

PII: S1359-8368(16)31436-6

DOI: 10.1016/j.compositesb.2017.01.032

Reference: JCOMB 4843

To appear in: *Composites Part B*

Received Date: 27 July 2016

Revised Date: 19 October 2016

Accepted Date: 25 January 2017

Please cite this article as: Kang W-S, Rhee KY, Park S-J, Influence of surface energetics of graphene oxide on fracture toughness of epoxy nanocomposites, *Composites Part B* (2017), doi: 10.1016/j.compositesb.2017.01.032.

This is a PDF file of an unedited manuscript that has been accepted for publication. As a service to our customers we are providing this early version of the manuscript. The manuscript will undergo copyediting, typesetting, and review of the resulting proof before it is published in its final form. Please note that during the production process errors may be discovered which could affect the content, and all legal disclaimers that apply to the journal pertain.

ACCEPTED MANUSCRIPT

Manuscript submitted to "*Composites Part B: Engineering*"

Influence of surface energetics of graphene oxide on fracture toughness of epoxy nanocomposites

Woo-Seok Kang[a], Kyong Yop Rhee[b, **], and Soo-Jin Park[a, *]

[a]*Department of Chemistry, Inha University, 100 Inharo, Incheon, Republic of Korea*

[b]*Department of Mechanical Engineering, College of Engineering, Kyung Hee University, Yongin 446-701, Republic of Korea*

[a, *]Corresponding author; Tel.: +82-32-876-7234; fax: +82-32-867-5604.

[b,**]Corresponding author. Tel.: +82-31-201-2565; Fax: +82-31-202-6693.

E-mail address: rheeky@khu.ac.kr (K.Y. Rhee), sjpark@inha.ac.kr (S. -J. Park)

ACCEPTED MANUSCRIPT

Abstract

The effects of the addition of graphene oxide (GO) as a filler for an epoxy matrix have been studied in terms of the surface energy and mechanical interfacial properties of GO/epoxy nanocomposites. The GO surface properties were determined using X-ray photoelectron spectroscopy and Fourier-transform infrared spectroscopy, and . The contact angle was measured by the sessile drop method for the evaluation of surface free energy. The investigated mechanical properties of the nanocomposites included the impact strength, fracture toughness and fracture energy. For the GO-reinforced epoxy resin matrix system, a direct linear relationship was observed between the specific polar components of the surface energy and the mechanical behavior. These results indicate that the mechanical interfacial properties of the GO/epoxy nanocomposites were controlled by the specific polar component including the electron–acceptor and electron–donor parameters.

***Keywords**: A. Resins; B. Fracture toughness; B. Surface properties.*

ACCEPTED MANUSCRIPT

1. Introduction

An increasing number of materials are currently being produced using filler-reinforced composites [1]. Epoxy-based materials are extensively used in polymer engineering, e.g., in cryogenic fuel tanks, coating agents for space shuttles, structural adhesives, microelectronics and matrix materials for structural composites. These materials possess many useful properties such as relatively good thermal stability combined with excellent stiffness, strength and excellent adhesion [2, 3]. However, the cured epoxy of the tight three-dimensional network structures is prone to fracture and exhibits a high cross-link density because of its inherent brittleness and poor crack resistance. Accordingly, numerous attempts have been made to improve the brittleness of these resins by adding various nanosized fillers, such as silica, carbon-based materials, clay, and inorganic particles to epoxy matrices. In addition, their combination has been used to enhance the fracture toughness, stiffness, and strength and even endow these materials with multifunctional properties [4–8].

Currently, carbon-based materials have been researched on their physicochemical, thermal stability, electrical and mechanical properties. Various carbon

ACCEPTED MANUSCRIPT

materials have emerged as potential fillers for polymer composites. The addition of carbon-based fillers, such as carbon black, carbon nanotubes, carbon fiber, expanded graphite and graphene have resulted in beneficial chemical and physical properties when employed in various applications. In several studies, carbon fillers have been successfully dispersed into epoxy resins, improving the fracture toughness and heat resistance and reducing the coefficient of thermal expansion [9–12].

Among these materials, graphene oxide (GO) has recently received considerable attention. GO consists of a single atomic layer of sp^2 carbon atoms. Commonly, graphite is oxidized to GO and is then chemically or thermally reduced to produce functionalized graphite. GO is a promising candidate filler for use in composites because of its high surface area, various reaction sites, low density, high thermal resistance, and good conductivity. In addition, during the oxidation of graphite, various oxygen-containing functional groups such as epoxides, hydroxyls, ketones and quinones are incorporated into the layers. The presence of functional groups improves the compatibility of graphite with various matrix polymers and promotes the dispersion of graphite in epoxy, organic solvents and water, yielding excellent mechanical and thermal properties. Therefore, GO is a considerably efficient filler. GO has been used as a nanosized filler in a wide range of polymer matrices including polyetherimide,

ACCEPTED MANUSCRIPT

polyurethane, and polypropylene. GO has also been investigated as a reinforcement in polymer composites [13–17].

The wettability of a solid surface describes the ability of a liquid to maintain contact with the surface, which is significant in the adherence or bonding of two materials. Additionally, the surface energetics of solid surfaces are critical in composite systems, as they can determine the strength of the solid surface interaction with its environment. Wettability, which depends on both roughness and chemical heterogeneity, is an important characteristic. A prerequisite for good adhesion between a filler and polymer is that the surface energy of the filler must be greater than or equal to that of the polymer. Pristine carbon exhibits a small surface energy and is unable to form strong adhesive bonds with polymers. However, various functional groups provide the GO film with high surface free energy, improving its wettability. The functional groups and energetic properties of GO can lead to completely different mechanical properties of the resulting composites. However, a systematic study of the effects of the addition of GO on both the surface energetics of GO and the mechanical interfacial properties of GO/polymer composites has yet to be comprehensively undertaken [18–23].

In this work, GO was used as a carbon filler to improve the mechanical interfacial properties of epoxy composites, and the correlation between the surface free

ACCEPTED MANUSCRIPT

energy and toughness behaviors of the resulting nanocomposites was investigated.

2. Experimental

2.1. Materials

Natural graphite particles with an average diameter of 500 μm were purchased from Sigma–Aldrich Co., Korea. The diglycidyl ether of bisphenol-A (DGEBA) type epoxy (YD-128) with an epoxide equivalent weight of 185–190 $g \cdot eq^{-1}$ and a density of approximately 1.16 $g \cdot cm^{-3}$ at 25 °C was supplied by Kukdo Chemical Co., Korea. The hardener used was 4,4'-diaminodiphenylmethane (DDM), supplied by TCI Co., Japan. Phosphoric acid (60%) and sulfuric acid (98 %) were supplied by Daejung Chemicals, Co., Korea.

2.2. Synthesis of GO

GO was prepared using Hummers' method with some modifications [24, 25]. Flake graphite was added to a 1:9 mixture of concentrated phosphoric acid/sulfuric acid with stirring; the mixture was then cooled under an ice bath, and the temperature was

ACCEPTED MANUSCRIPT

maintained below 20 °C. Subsequently, $KMnO_4$ was added with stirring, and the reaction was allowed to proceed at 45 °C for 24 h. In the next step, the mixture was cooled down to ambient temperature and poured onto ice (~ 400 mL); 30% hydrogen peroxide was slowly added to the mixture, which was maintained at the same temperature. Subsequently, the solution was filtered and washed repeatedly with 10% hydrogen chloride, ethanol, and distilled water until a neutral pH was reached. The mixture was then dispersed in distilled water using ultrasonication, and the GO powder was prepared by freeze drying. Finally, the GO powder was vacuum dried for 6 h at room temperature.

2.3. Fabrication of epoxy composites with GO

Epoxy composites containing GO were prepared using the following procedure. GO was first dispersed in acetone by sonication at ambient temperature for 30 min. The solution was then mixed with the epoxy by sonication for 30 min. Then, the mixture was degassed at 80 °C in a vacuum oven for 6 h to remove the solvent. Subsequently, the addition of the curing agent with DDM was performed using mechanical mixing for

ACCEPTED MANUSCRIPT

30 min. The bubble-free mixture was then poured into a preheated mold. Finally, the curing steps were performed in a convection oven at 130 °C for 1 h, 150 °C for 2 h, and 170 °C for 1 h. Composites containing different weight ratios (0.25, 0.5, 1.0, 1.5, and 2.0 wt%) of as-received GO were prepared. The preparation route for the GO/epoxy nanocomposites is illustrated in Fig. 1.

2.4. Characterization and measurements

The structural properties were examined using X-ray diffraction (XRD, D2 PHASER, Bruker Co.). Infrared spectra were obtained using Fourier-transform infrared spectroscopy (FT-IR, PS-4000, Jasco Co.). The surface properties of the specimens were determined using X-ray photoelectron spectroscopy (XPS, K-Alpha, Thermo Scientific Co.). The thermal properties were analyzed using a thermogravimetric analyzer (TGA, Model TG209F3, Netzsch Co.). The morphologies and microstructures of the prepared composites were examined using field-emission transmission electron microscopy (FE-TEM, JEM-2100F, JEOL Co., Ltd.), atomic force microscopy (AFM, Nanoscope Multimode IVa, Bruker Co.), and high-resolution scanning electron microscopy (HR-

ACCEPTED MANUSCRIPT

135 SEM, Model SU-8010, Hitachi Co., Ltd.).

136 The contact angle was measured using the sessile drop method on a Rame–Hart
137 goniometer (Phoenix 300 Plus, SEO Co.). A wetting liquid (5 μL) was used for each
138 evaluation at 25 ± 1 °C, and more than 10 drops were tested for each prepared
139 composite. Contact angle measurements were performed within 5 s of contact for the
140 critical surface tension. In this work, three different wetting liquids were selected:
141 distilled water, diiodomethane, and ethylene glycol. The interfacial (or surface) tension,
142 London dispersion force, and specific (or polar) components were analyzed to
143 determine their components, including the acid and base parameters of the surface free
144 energy. The basic characteristics of the surface free energy of the liquids are listed in
145 Table 1 and were used to evaluate the surface free energies of the casting surfaces [26].
146 The data were averaged for 10 specimens.

147 Izod impact tests were performed on notched specimens using an impact testing
148 machine (BESTIPT-320I, Ssaul Bestech Co.) according to ASTM D-256. The specimen
149 size was $5 \times 12.7 \times 63.5$ mm^3. The critical stress intensity factor (K_{IC}) and critical strain
150 energy release rate (G_{IC}) of the prepared composites were measured using single-edge-
151 notched specimens; the tests were performed with a universal test machine (UTM,

ACCEPTED MANUSCRIPT

LR5KPlus, Lloyd Instruments Ltd.) according to ASTM E-399. The sample size was 5 × 10 × 50 mm^3, and the cross-head speed was 0.85 $mm \cdot min^{-1}$. The data were averaged for five specimens.

3. Results and discussion

3.1. Morphology and characterization of GO

Fig. 2 presents TEM and AFM images of GO. The TEM image in Fig. 2a reveals a large area of a GO sheet exhibiting a transparent clean surface and a few thin ripples, which indicates that the surface functionalization successfully changed the surface morphology of the GO sheets. The formation of GO with a wrinkled surface is often considered beneficial for a strong interfacial interaction with the polar epoxy matrix. The morphology and thickness of the GO sheets was investigated using AFM, which offers immediate evidence for ultra-thin nano-sheets (Fig. 2c). The size of GO mainly ranged from 0.25 to 5.0 μm with an average thickness of approximately 0.927 nm, indicating the presence of one-atom-thick GO due to the sonication-assisted exfoliation [27].

ACCEPTED MANUSCRIPT

The various GO functional groups were examined using FT-IR spectroscopy and XPS. Fig. 3a presents FT-IR spectra of the pristine graphite and GO, which were consistent with the data reported in the literature [28, 29]. After modification, a series of new peaks appeared. The peaks at 3360, 1682, and 1037 cm^{-1} indicate that the GO surface was covered with hydroxyl (–OH), carbonyl/ester (–C=O), and hydroxyl/ether (–C–O) groups, respectively, which were formed during the oxidation process in the chemical exfoliation. These results indicate that the O-containing groups were successfully introduced onto the graphite surfaces. The XPS spectra were analyzed to further identify the surface chemical compositions and their changes with the GO content. The C1s core level spectrum of GO is shown in Fig. 3b. As previously reported in the literature, GO exhibited six different chemically shifted components: sp^2 C=C (284.5 eV), sp^3 C–C/C–H (284.8 eV), C=OH (285.3 eV), C–O–C (286.7 eV), C=O (287.1 eV), and O–C=O (288.6 eV), confirming the successful modification based on pristine graphite. Thus XPS and FT-IR spectra demonstrate the presence of different types of oxygen functional groups on the surface of GO, which could affect the cure reaction of the epoxy resin.

The interlayer distance (d002) was calculated from the C (002) peak of the XRD pattern using Bragg's law:

ACCEPTED MANUSCRIPT

$$n\lambda = 2d\sin\theta \quad (1)$$

where n is an integer, θ is the X-ray wavelength, d is the interlayer distance, and λ is the diffraction angle.

XRD patterns of the GO and pristine graphite are presented in Fig. 3c. The XRD patterns of the pristine graphite reveal an intense diffraction (002) peak at 2θ = 26.6°, reflecting a d-spacing of 0.335 nm between the graphitic interlayers. A well-defined GO diffraction peak was observed at 2θ = 11.03°, indicating that the interlayer spacing or gap increased to 0.801 nm. This result confirmed that GO was exfoliated into stacking layered sheets, which is in good agreement with previous results [30].

Fig. 3d presents the TGA curves of the pristine graphite and GO. The pristine graphite exhibited high thermal stability and did not decompose up to 600 ℃. The degradation curve of GO indicates a two-stage process in atmosphere. A similar pattern was observed by Wan et al. and Shen et al. [28, 31]. The first weight loss occurred below 100 ℃ because of the vaporization of water and other volatile impurities. The second stage occurred between approximately 200 and 500 ℃ because of the pyrolysis of unstable oxygen functional groups such as carbonyl, hydroxyl, and carboxylic groups, which caused the generation of gases including CO, CO_2, and steam.

ACCEPTED MANUSCRIPT

3.2. Structural characterization of GO/epoxy nanocomposites

The inner structures of the GO/epoxy nanocomposites were examined using TEM. Fig. 4a reveals the homogenous and uniform dispersion of GO sheets with an intercalated-exfoliated and hair-like structure without aggregates and single or ultrathin sheets with a thickness of less than several nanometers, demonstrating the high compatibility between GO and the epoxy matrix to achieve nanoscale dispersion. Consequently, by analyzing the nanocomposite morphology, the layered structure of the GO filler, which is supposed to improve the mechanical properties, could be observed. However, some bundles and stacks appeared when the content of GO exceeded 1.00 wt% (Figs. 4b and c); because of the increase in the GO content, the agglomerates became denser, hindering the dispersion of GO in the polymer matrix (Figs. 4b and c, black arrows). Notably, the interfacial bonding between GO and the epoxy matrix was not ideal, leading to degradation of the mechanical properties [27].

Fig. 5 presents SEM images of the prepared composites after the K_{IC} tests. Fig. 5a reveals that the fracture surface of DGEBA was smooth and mirror-like. The cracks spread freely and randomly, which is typical of brittle fracture and demonstrates the poor impact strength of the neat epoxy. In contrast, the prepared composites containing GO exhibited rough fracture surfaces (Figs. 5b–f), which indicated the need of a large

ACCEPTED MANUSCRIPT

222 amount of energy during crack propagation and resulted in a high impact strength and
223 fracture toughness. Fig. 5d shows that GO was uniformly dispersed in the epoxy resin.
224 In addition, rough fracture surfaces with numerous tortuous and fine river-like structures
225 were observed because of the embedding of GO sheets in the epoxy matrix. This finding
226 provides clear evidence of the strong interaction between the GO sheet and epoxy
227 matrix. The large surface area and presence of multifunctional groups increased the
228 interfacial adhesion between the filler and matrix, leading to a significant improvement
229 of the mechanical properties, which was reflected in the fracture surface of the
230 composites. Notably, agglomerates, which reduced the mechanical properties of the
231 epoxy matrix, can be observed in Figs. 5e and f [32].
232
233 *3.3. Surface energy*
234 The adsorption (gas–solid), wettability (liquid–solid), adhesion (solid–solid),
235 and morphology of the component phases were greatly affected by the interfacial and
236 surface free energy, which is important in evaluating the physical and mechanical
237 properties of the composites. The surface free energy of the composites was calculated
238 based on the contact angle formed between the liquid and a solid of known surface free
239 energy. According to Fowkes, Owens, and Wu, the total surface free energy can be

ACCEPTED MANUSCRIPT

240 divided into two components [33–35]:

241 $$\gamma = \gamma^{L} + \gamma^{SP} \quad (2)$$

242 where γ^{L} is the dispersive component of the surface free energy related to Lifshitz–
243 van der Waals interactions that encompass London dispersion forces, and γ^{SP} is the
244 specific polar component of the surface free energy related to Debye-inductive
245 polarization, Keeson forces, van der Waals forces, and hydrogen bonding.

246 The γ^{SP} component results from electron–acceptor and electron–donor
247 intermolecular interactions, called Lewis acid and base interactions, respectively. The
248 term γ^{SP} is further divided into two parameters using the geometric mean:

249 $$\gamma^{SP} = 2\sqrt{\gamma^{+} \cdot \gamma^{-}} \quad (3)$$

250 where γ^{+} represents the electron–acceptor parameter and γ^{-} represents the electron–
251 donor parameter. The surface free energy of the solid (γ_S) is calculated using the
252 following equation based on van der Waals acid–base parameters:

253 $$\gamma_{L,i}(1+\cos\theta) = 2\left(\sqrt{\gamma_S^{L} \cdot \gamma_{L,i}^{L}} + \sqrt{\gamma_S^{+} \cdot \gamma_{L,i}^{-}} + \sqrt{\gamma_S^{-} \cdot \gamma_{L,i}^{+}}\right) \quad (4)$$

254 where γ_L is the experimentally analyzed surface tension of the liquid, θ is the contact

ACCEPTED MANUSCRIPT

255 angle, and the subscripts S and L refer to the solid and liquid phases, respectively. The
256 subscript *i* indicates the experimental testing liquid, i.e., in this work, water,
257 diiodomethane, and ethylene glycol.

258 Knowing the values of γ_L^L, γ_L^+, and γ_L^- for the three liquids and their contact
259 angles on the solid (θ), a set of Eq. (4) can be simultaneously solved to determine the
260 surface free energy parameters for the solid, γ_S^L, γ_S^+, and γ_S^-. Table 2 summarizes the
261 results of the London dispersive component and specific component, including the
262 contact angle of the prepared composites for the surface free energy [20, 26].

263 The contact angles of the test liquids (distilled water, diiodomethane, and
264 ethylene glycol) on the prepared composites were measured using Young's equation. Fig.
265 6 presents schematic diagrams illustrating the variations of the contact angle and surface
266 properties of the GO/epoxy nanocomposites. The wettability of the prepared composites
267 was assessed by evaluating the contact angle of a sessile droplet of three different
268 liquids on the surfaces. The surfaces of the composites were determined to be
269 hydrophilic if the water contact angle was in the range of $0° \leq \theta < 90°$ and hydrophobic
270 if the water angle was in the range of $90° < \theta \leq 180°$. As observed in Fig. 6a, the
271 distilled water droplet retained an ellipsoidal shape on the neat epoxy, with a contact

ACCEPTED MANUSCRIPT

angle of 75.20° ± 2°, suggesting that the neat epoxy materials had a relatively hydrophilic character. A sharp decrease in the contact angle of the prepared composites from 75.20° to 55.24° was observed upon increasing the GO ratio (Fig. 6). These results indicate that the GO surface retained the hydrophilic properties of the various functional groups. Upon the addition of GO, the contact angle changed more severely for the polar-elemental distilled water. This result indicates that among the properties of GO, the specific component on the surface had a greater effect than the London dispersion component [36, 37].

Surface energy is directly related to the adhesion force, assuming that the strength of adhesive bonding is proportional to the work of adhesion. The interfacial tension and surface free energy values for the prepared composites are reported in Table 2. GO exhibited the maximum total surface free energy, mainly because of its impressive specific polar components, γ_S^{SP}, which involved increases in both parameters of the specific polar component of surface free energy, γ_S^+ and γ_S^-. Table 2 lists the γ_S^+ and γ_S^- components of the specific polar component. The filler addition led to a systematic increase in the γ^+ values of the prepared composites with respect to that of the neat epoxy resin, indicating that the increase in the γ_S^+ component of the

ACCEPTED MANUSCRIPT

surface free energy could be largely attributed to the polar basic surface functional groups on the GO sheet. In addition, a major portion of the interfacial interaction was due to intermolecular acid-base interactions at the interfaces between the matrix and GO. Notably, the polar component was dependent on the surface activity, which was related to the surface functional groups, i.e., hydroxyl, carbonyl, carboxyl, and ether groups. This interfacial tension increase could be attributed to intermolecular hydrogen bonding between the GO and epoxy resin, which is one of the factors affecting the specific polar component of the surface free energy, as demonstrated by the FT-IR and XPS results in Fig. 3. The specific polar component had a more significant effect on the surface free energy than the London dispersive component. The surface free energy increased upon increasing the GO content to 1.0 wt%. However, when the GO content exceeded 1.00 wt%, GO tended to excessively bond with itself, rather than with the epoxy resin because of its large surface area and strong van der Waals force. This phenomenon generated a lengthened grafted chain that formed agglomerates (Fig. S1), preventing the formation of a tight bridge structure and reducing the binding force, thus leading to a decrease of the surface free energy [26, 38]. The agglomeration and tight bridge structure in epoxy matrix are illustrated in Fig. 7.

ACCEPTED MANUSCRIPT

3.4. Mechanical behavior

The mechanical properties of the composites, including their impact strength and fracture toughness, were investigated, and K_{IC} and G_{IC} were determined. The value of K_{IC} was calculated as follows [39, 40]:

$$K_{IC} = \frac{L \cdot P}{bd^{3/2}} Y \tag{5}$$

Here, L is the length of the span (mm), P is the critical load for crack propagation, d is the specimen thickness (mm), b is the specimen width (mm), and Y is the geometrical factor given by Eq. 6 with a being the pre-crack length (mm):

$$Y = \frac{3a/d^{1/2}[1.99-(a/d)(1-a/d)(2.15-3.93a/d+(2.7a^2)/b^2)]}{2(1+2a/d)(1-a/d)^{3/2}} \tag{6}$$

G_{IC} was calculated using K_{IC} and the following equation [41]:

$$G_{IC} = \frac{(1-v^2)\cdot K_{IC}^2}{E} \tag{7}$$

where v is Poisson's ratio of the epoxy resin, taken to be 0.3 [42], and E is the tensile modulus acquired from fracture testing.

Fig. 8a shows the impact strength of the GO/epoxy nanocomposites. The epoxy

ACCEPTED MANUSCRIPT

resin was brittle, exhibiting an impact strength of 4.01 ± 0.3 kJ·m^{-2}, whereas the impact strength of the prepared nanocomposite containing GO was nearly 80% higher at 7.24 ± 0.2 kJ·m^{-2}. The addition of GO enhanced the impact strength of the composites because of the strong hydrogen bonding between the GO functional groups and epoxy matrix. In contrast, an increase in the mass ratio of GO (1.0 wt%) led to the formation of agglomerates in the epoxy network. The presence of agglomerates led to low interfacial adhesion between the filler and epoxy, thereby reducing the impact strength. The various GO surface functional groups enhanced the adhesion and chemical bonding, which improved the energy absorption during impact loading. In addition, these findings indicate that the well-dispersed GO sheets were considerably more effective than the poorly dispersed sheets in improving the impact strength of the epoxy resin [43].

Fig. 8b shows the K_{IC} and G_{IC} values. K_{IC} and G_{IC} of the neat epoxy were 1.39 ± 0.10 MPa·m$^{1/2}$ and 4.48 ± 1.20 kJ·m^{-2}, respectively, which are typical values for brittle epoxy materials [44–46]. As expected, the addition of GO as a filler effectively improved the K_{IC} and G_{IC} values. The fracture toughness of the prepared nanocomposites was enhanced by increasing the GO ratio. The K_{IC} and G_{IC} values of

ACCEPTED MANUSCRIPT

the prepared composites exhibited maximum values at 1.0 wt% GO. The K_{IC} value at 1 wt% GO content, 2.76 ± 0.17 MPa·m$^{1/2}$, was 98% higher than that of the neat epoxy. Notably, the presence of GO in the matrix could lead to crosslinking through chemical bonding, such as hydrogen bonding between the epoxide groups of the epoxy resin and various surface functional groups of GO, thereby increasing the critical energy release and fracture toughness values. In contrast, a further increase in the mass ratio of GO beyond 1.0 wt% led to the formation of micron-scale agglomerates within the epoxy network due to the strong van der Waals force of GO, which caused a deterioration of the mechanical interfacial properties of the epoxy nanocomposites [41, 47]. Therefore, a better dispersion of GO fillers in the matrix could have led to crosslinking through chemical bonding, thereby increasing the critical energy release and fracture toughness values.

In addition, the mechanical properties and surface energy of the prepared composites are plotted in Fig. 9. Both graphs reveal good linearity (regression coefficients of R^2 = 0.9615 and 0.9881, respectively) for the relationship between γ^{SP} of the surface free energy and the mechanical interfacial properties, such as K_{IC} and impact strength. This result is similar to those presented in previous reports [48],

ACCEPTED MANUSCRIPT

355 indicating that an increase in the specific polar component of the surface free energy is
356 important in enhancing the physical GO filler–epoxy matrix of the prepared
357 nanocomposites.

358

359 **4. Conclusions**

360 This study demonstrated that increasing the amount of GO filler leads to an
361 improvement of the impact strength and K_{IC} value of GO/epoxy composites. Relative to
362 the neat epoxy resin, the addition of 1.00 wt% GO resulted in an 80% increase of the
363 impact strength (from 4.01 ± 0.3 to 7.24 ± 0.2 $kJ \cdot m^{-2}$) and 98% increase of the K_{IC}
364 value (from 1.39 ± 0.10 to 2.76 ± 0.17 $MPa \cdot m^{1/2}$). This finding indicates that increasing
365 the GO filler content led to an increase of the mechanical interfacial properties, mainly
366 because the GO hydroxyl groups improved the chemical bonding and caused a strong
367 interfacial interaction between the GO surface and epoxy matrix. This phenomenon
368 clearly resulted in an increase of the specific polar component of the surface free energy
369 for the intermolecular physical bonding properties among the three different elements of
370 the GO/epoxy nanocomposites. This increase in the specific polar component of the
371 surface free energy consequently plays an important role in improving the degree of
372 adhesion at interfaces in the nanocomposite system.

ACCEPTED MANUSCRIPT

Acknowledgments

This work was supported by the Korea Institute of Energy Technology Evaluation and Planning (KETEP) and the Ministry of Trade, Industry & Energy (MOTIE) of the Republic of Korea (20153030031710).

ACCEPTED MANUSCRIPT

ACCEPTED MANUSCRIPT

References

[1] Stankovich S, Dikin DA, Dommett GH, Kohlhaas KM, Zimney EJ, Stach EA, Ruoff RS. Graphene-based composite materials. Nature 2006;442:282-6.

[2] Chrusciel JJ, Lesniak E. Modification of epoxy resins with functional silanes, polysiloxanes, silsesquioxanes, silica and silicates. Prog Polym Sci 2015;41:67-121.

[3] Huang L, Yi N, Wu Y, Zhang Y, Zhang Q, Huang Y, Chen Y. Multichannel and repeatable self-healing of mechanical enhanced graphene-thermoplastic polyurethane composites. Adv Mater 2013;25:2224-8.

[4] Gómez-del Río T, Salazar A, Pearson RA, Rodríguez J. Fracture behaviour of epoxy nanocomposites modified with triblock copolymers and carbon nanotubes. Compos Part B–Eng 2016;87:343-9.

[5] Park SJ, Jin FL. Thermal stabilities and dynamic mechanical properties of sulfone-containing epoxy resin cured with anhydride. Polym Degrad Stab 2004;86:515-20.

[6] Bruce AN, Lieber D, Hua I, Howarter JA. Rational interface design of epoxy–organoclay nanocomposites: Role of structure-property relationship for silane modifiers. J colloid Interf Sci 2014;419:73-8.

[7] Wang Z, Huang X, Bai L, Du R, Liu Y, Zhang Y, Zhao G. Effect of micro-Al2O3 contents on mechanical property of carbon fiber reinforced epoxy matrix composites. Compos Part B-Eng 2016;91:392-8.

[8] Park SJ, Park WB, Lee JR. Roles of unsaturated polyester in the epoxy matrix system. Polym J 1999;31:28-31.

[9] Moriche R, Sánchez M, Jiménez-Suárez A, Prolongo SG, Ureña A. Electrically conductive functionalized-GNP/epoxy based composites: From nanocomposite to multiscale glass fibre composite material. Compos Part B–Eng 2016;98:49-55.

[10] Zhang XC, Scarpa F, McHale R, Peng HX. Poly (methyl methacrylate)-decorated single wall carbon nanotube/epoxy nanocomposites with re-agglomeration networks: Rheology and viscoelastic damping performance. Polymer 2016;87:236-45.

ACCEPTED MANUSCRIPT

[11] Lee MW, Wang TY, Tsai JL. Characterizing the interfacial shear strength of graphite/epoxy composites containing functionalized graphene. Compos Part B–Eng 2016;98:308-13.

[12] Jin FL, Li X, Park SJ. Synthesis and application of epoxy resins: A review. J Ind Eng Chem 2015;29:1-11.

[13] Yadav M, Rhee KY, Park SJ, Hui D. Mechanical properties of Fe3O4/GO/chitosan composites. Compos Part B-Eng 2014;66:89-96.

[14] Radic S, Geitner NK, Podila R, Käkinen A, Chen P, Ke PC, Ding F. Competitive binding of natural amphiphiles with graphene derivatives. Sci Rep 2013;3:2273-10.

[15] Jiang SD, Bai ZM, Tang G, Hu Y, Song L. Fabrication and characterization of graphene oxide-reinforced poly (vinyl alcohol)-based hybrid composites by the sol–gel method. Compos Sci Technol 2014;102:51-8.

[16] Li P, Zheng Y, Shi T, Wang Y, Li M, Chen C, Zhang J. A solvent-free graphene oxide nanoribbon colloid as filler phase for epoxy-matrix composites with enhanced mechanical, thermal and tribological performance. Carbon 2016;96: 40-8.

[17] Chen L, Li W, Liu Y, Leng J. Nanocomposites of epoxy-based shape memory polymer and thermally reduced graphite oxide: Mechanical, thermal and shape memory characterizations. Compos Part B–Eng 2016;91:75-82.

[18] Dingreville R, Qu J, Cherkaoui M. Surface free energy and its effect on the elastic behavior of nano-sized particles, wires and films. J Mech Phys Solids 2005;53:1827-54.

[19] Meng LY, Park SJ. Superhydrophobic carbon-based materials: a review of synthesis, structure, and applications. Carbon Lett 2014;15:89-104.

[20] Park SJ, Kim BJ, Seo DI, Rhee KY, Lyu YY. Effects of a silane treatment on the mechanical interfacial properties of montmorillonite/epoxy nanocomposites. Mat Sci Eng A-Struct 2009;526:74-8.

[21] Wang S, Zhang Y, Abidi N, Cabrales L. Wettability and surface free energy of graphene films. Langmuir 2009;25:11078-81.

[22] Nejad HB, Baker RM, Mather PT. Preparation and characterization of triple shape memory composite foams. Soft Matter 2014;10:8066-74.

[23] Lee W, Lee JU, Byun JH. Catecholamine polymers as surface modifiers for enhancing interfacial strength of fiber-reinforced composites. Compos Sci Technol 2015;110:53-61.

ACCEPTED MANUSCRIPT

[24] Offeman RE, Hummers WS. Preparation of graphitic oxide. J Am Chem Soc 1958;80:1339.

[25] Marcano DC, Kosynkin DV, Berlin JM, Sinitskii A, Sun Z, Slesarev A, Tour JM. Improved synthesis of graphene oxide. ACS nano 2010;4:4806-14.

[26] Park SJ, Seo MK, Nah C. Influence of surface characteristics of carbon blacks on cure and mechanical behaviors of rubber matrix compoundings. J Colloid Interf Sci 2005;291:229-35.

[27] Bao C, Guo Y, Song L, Kan Y, Qian X, Hu Y. In situ preparation of functionalized graphene oxide/epoxy nanocomposites with effective reinforcements. J Mater Chem 2011;21:13290-8.

[28] Wan YJ, Gong LX, Tang LC, Wu LB, Jiang JX. Mechanical properties of epoxy composites filled with silane-functionalized graphene oxide. Compos Part-A-Appl 2014;64:79-89.

[29] Yue W, Lin Z, Jiang S, Yang X. Preparation of graphene-encapsulated mesoporous metal oxides and their application as anode materials for lithium-ion batteries. J Mater Chem 2012;22:16318-23.

[30] Du FP, Wang JJ, Tang CY, Tsui CP, Zhou XP, Xie XL, Liao YG. Water-soluble graphene grafted by poly (sodium 4-styrenesulfonate) for enhancement of electric capacitance. Nanotechnology 2012;23:475704-13.

[31] Shen J, Yan B, Shi M, Ma H, Li N, Ye M. Synthesis of graphene oxide-based biocomposites through diimide-activated amidation. J Colloid Interf Sci 2011;356:543-9.

[32] Zaman I, Kuan HC, Dai J, Kawashima N, Michelmore A, Sovi A, Ma J. From carbon nanotubes and silicate layers to graphene platelets for polymer nanocomposites. Nanoscale 2012;4:4578-86.

[33] Fowkes FM. Determination of interfacial tensions, contact angles, and dispersion forces in surfaces by assuming additivity of intermolecular interactions in surfaces. J Phys Chem 1962;66:382.

[34] Owens DK, Wendt RC. Estimation of the surface free energy of polymers. J Appl Polym Sci 1969;13:1741-7.

[35] Park SJ, Seo MK. Interface science and composites (Vol. 18). Academic press;2011.

[36] Tang K, Yu J, Zhao Y, Liu Y, Wang X, Xu R. Fabrication of super-hydrophobic and super-oleophilic boehmite membranes from anodic alumina oxide film via a two-phase thermal approach. J Mater Chem 2006;16:1741-5.

ACCEPTED MANUSCRIPT

[37] Pietsch T, Gindy N, Fahmi A. Nano-and micro-sized honeycomb patterns through hierarchical self-assembly of metal-loaded diblock copolymer vesicles. Soft Matter 2009;5:2188-97.

[38] Zhao Q, Liu Y, Abel EW. Surface free energies of electroless Ni–P based composite coatings. Appl Surf Sci 2005;240:441-51.

[39] Tang LC, Wan YJ, Yan D, Pei YB, Zhao L, Li YB, Lai GQ. The effect of graphene dispersion on the mechanical properties of graphene/epoxy composites. Carbon 2013;60:16-27.

[40] Park SJ, Kim MH, Lee JR, Choi S. Effect of fiber–polymer interactions on fracture toughness behavior of carbon fiber-reinforced epoxy matrix composites. J Colloid Interf Sci 2000;228:287-91.

[41] Wang R, Li Z, Liu W, Jiao W, Hao L, Yang F. Attapulgite–graphene oxide hybrids as thermal and mechanical reinforcements for epoxy composites. Compos Sci Technol 2013;87:29-35.

[42] Kinloch AJ. Adhesion and adhesives: science and technology. Springer Science & Business Media;1987.

[43] Ni C, Ni G, Zhang L, Mi J, Yao B, Zhu C. Syntheses of silsesquioxane (POSS)-based inorganic/organic hybrid and the application in reinforcement for an epoxy resin. J Colloid Interf Sci 2011;362:94-9.

[44] Kang WS, Rhee KY, Park SJ. Thermal, impact and toughness behaviors of expanded graphite/graphite oxide-filled epoxy composites. Compos Part B–Eng 2016;94:238-44.

[45] Park YT, Qian Y, Chan C, Suh T, Nejhad MG, Macosko CW, Stein A. Epoxy toughening with low graphene loading. Adv Funct Mater 2015;25:575-85.

[46] Gong LX, Zhao L, Tang LC, Liu HY, Mai YW. Balanced electrical, thermal and mechanical properties of epoxy composites filled with chemically reduced graphene oxide and rubber nanoparticles. Compos Sci Technol 2015;121:104-14.

[47] Wan YJ, Tang LC, Gong LX, Yan D, Li YB, Wu LB, Lai GQ. Grafting of epoxy chains onto graphene oxide for epoxy composites with improved mechanical and thermal properties. Carbon 2014;69:467-80.

[48] Park SJ, Cho MS, Lee JR. Studies on the surface free energy of carbon–carbon composites: effect of filler addition on the ILSS of composites. J Colloid Interf Sci 2000;226:60-4.

ACCEPTED MANUSCRIPT

Figure Captions

Fig. 1 Schematic diagram of the preparation of GO/epoxy nanocomposites.

Fig. 2 Micrographs of GO sheets: (a) TEM image of GO, (b) magnified image of the boxed region in (a), and (c) AFM image of GO.

Fig. 3 Characterization of GO sheets: (a) FT-IR spectra, (b) C1s core level of XPS spectra, (c) XRD patterns, and (d) TGA curves.

Fig. 4 TEM images of GO/epoxy nanocomposites with different GO contents: (a) 1.00 wt%, (b) 1.50 wt%, and (c) 2.00 wt%.

Fig. 5 SEM images of cross-sectional fracture surfaces of GO/epoxy composites: (a) neat epoxy, (b) 0.25 wt%, (c) 0.50 wt%, (d) 1.00 wt%, (e) 1.50 wt%, and (f) 2.00 wt%.

Fig. 6 Illustrating the changes of water contact angle of the GO/epoxy nanocomposites: (a) neat epoxy, (b) 0.25 wt%, (c) 0.5 wt%, (d) 1.0 wt%, (e) 1.5 wt%, and (f) 2.0 wt%.

Fig. 7 Schematic diagram of agglomeration and tight bridge structure in epoxy matrix.

Fig. 8 Mechanical properties of GO/epoxy nanocomposites: (a) impact strength and (b) fracture toughness.

Fig. 9 Dependence of impact strength and K_{IC} of GO/epoxy nanocomposites on γ_s.

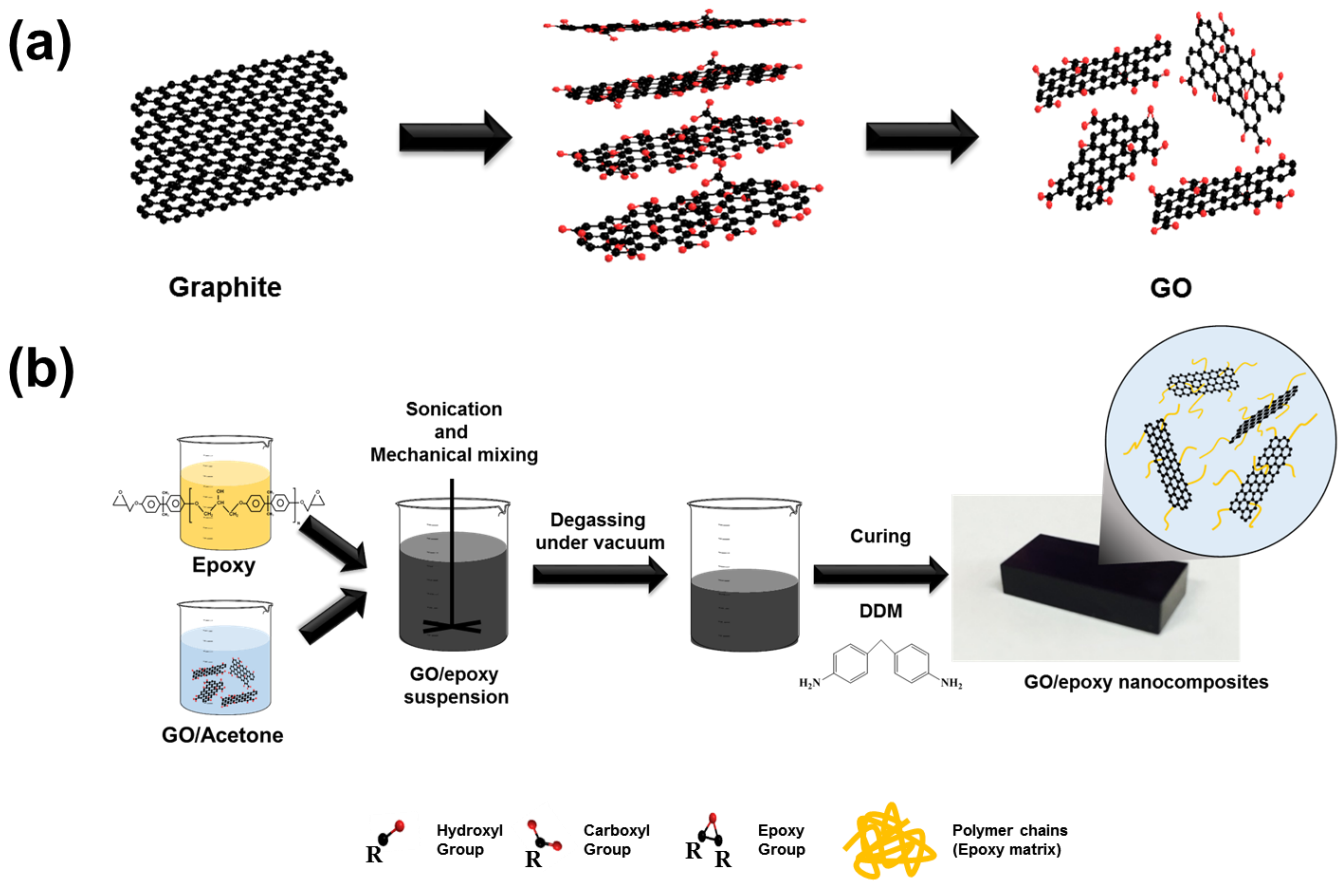

Fig. 1. Schematic diagram of the preparation of (a) GO and (b) GO/epoxy nanocomposites.

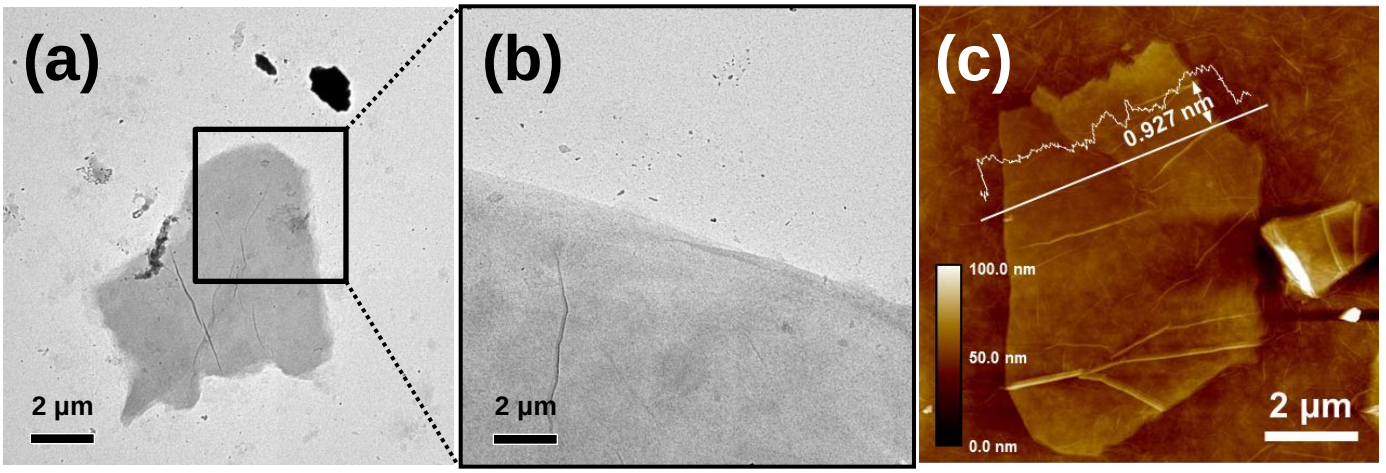

Fig. 2. Micrographs of GO sheets: (a) TEM image of GO, (b) magnified image of the boxed region in (a), and (c) AFM image of GO.

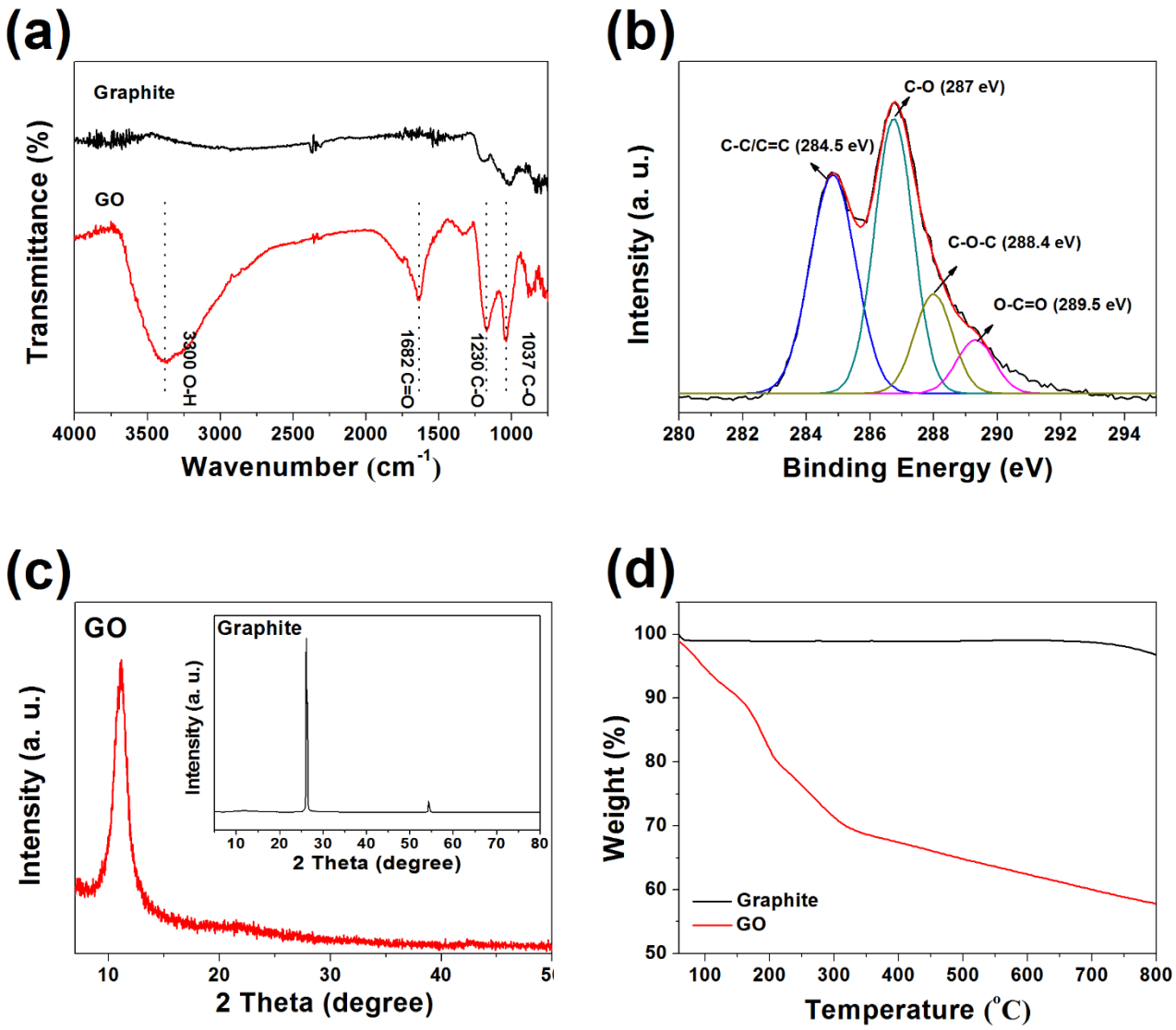

Fig. 3. Characterization of GO sheets: (a) FT-IR spectra, (b) C1s core level of XPS spectra, (c) XRD patterns, and (d) TGA curves.

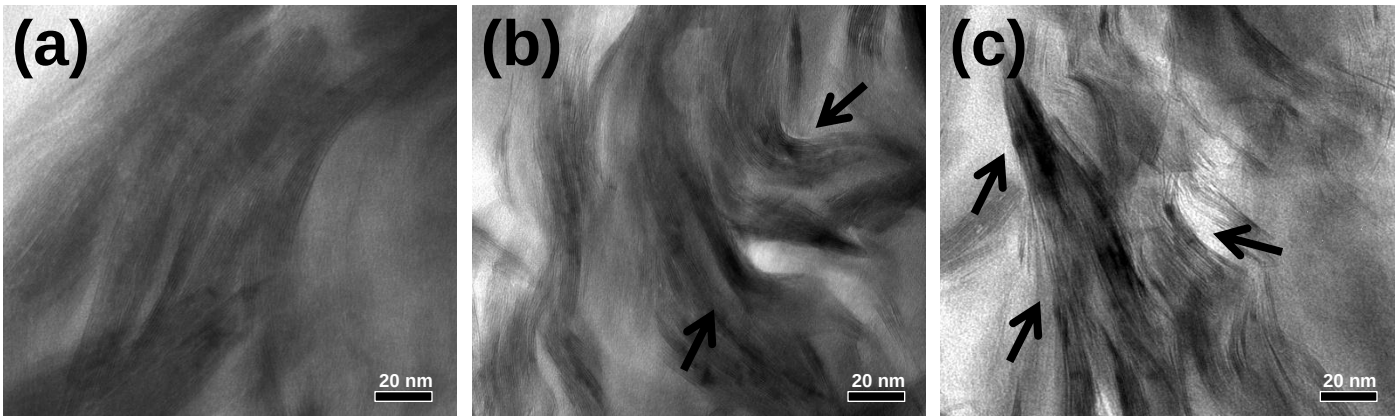

Fig. 4. TEM images of GO/epoxy nanocomposites different GO contents: (a) 1.0 wt%, (b) 1.5 wt%, and (c) 2.0 wt%.

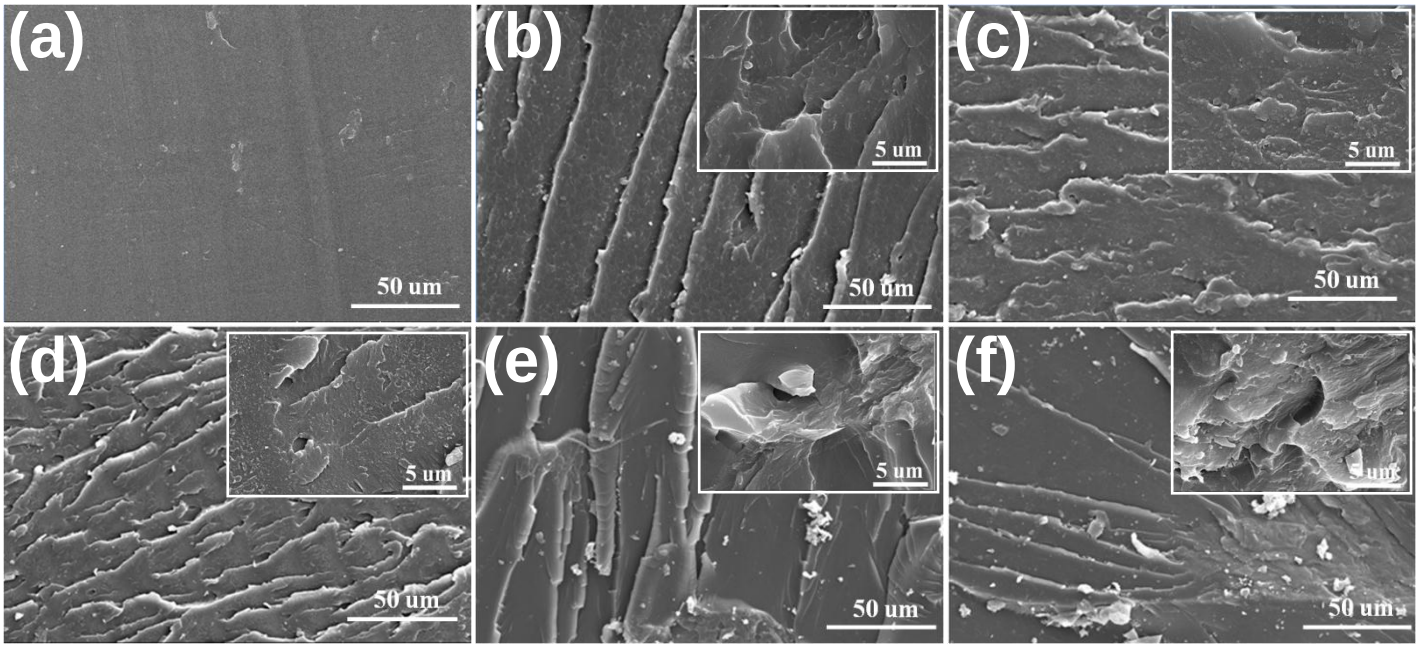

Fig. 5. SEM images of cross-sectional fracture surfaces of GO/epoxy composites: (a) neat epoxy, (b) 0.25 wt%, (c) 0.50 wt%, (d) 1.00 wt%, (e) 1.50 wt%, and (f) 2.00 wt%.

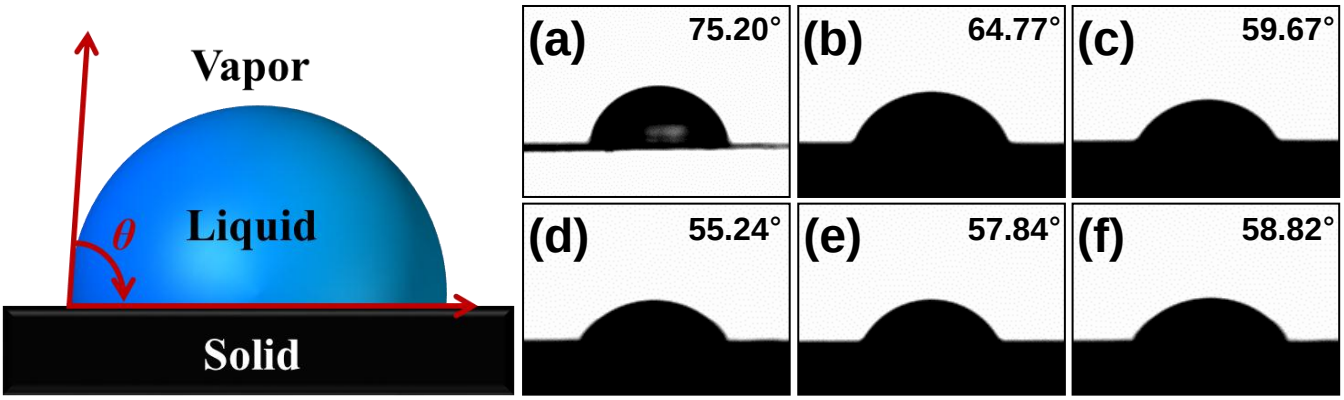

Fig. 6. Illustrating the changes of water contact angle of the GO/epoxy nanocomposites: (a) neat epoxy, (b) 0.25 wt%, (c) 0.5 wt%, (d) 1.0 wt%, (e) 1.5 wt%, and (f) 2.0 wt%.

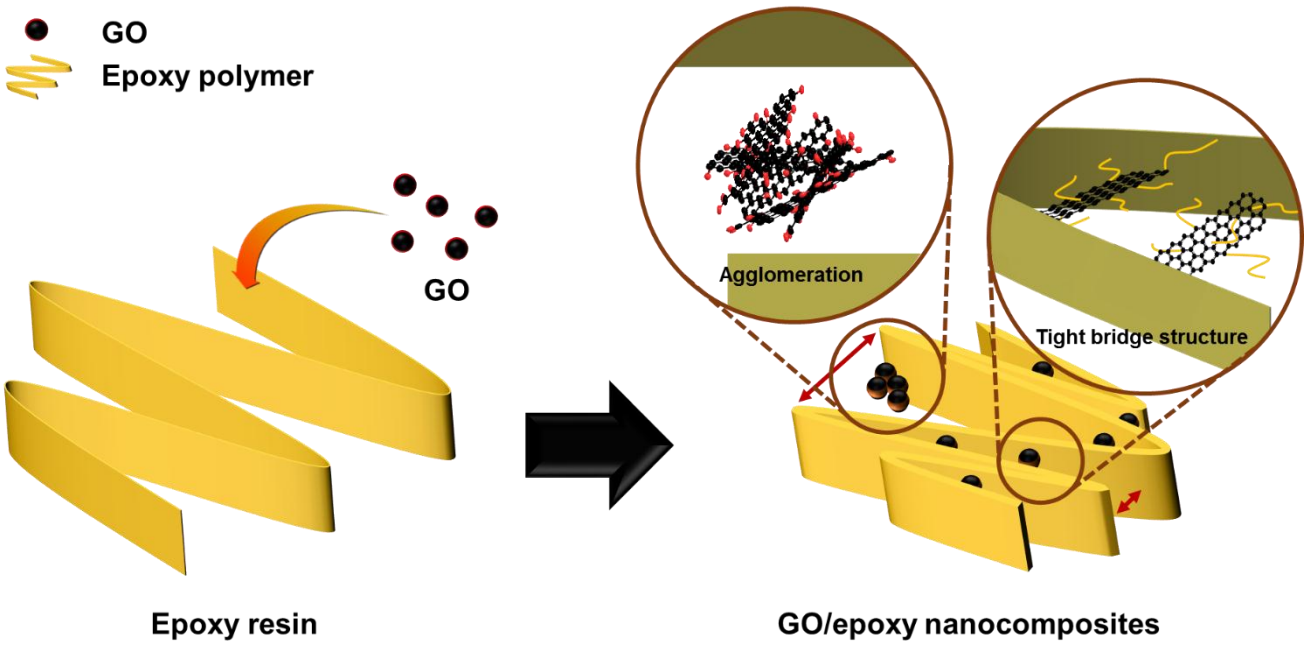

Fig. 7. Schematic diagram of agglomeration and tight bridge structure in epoxy matrix.

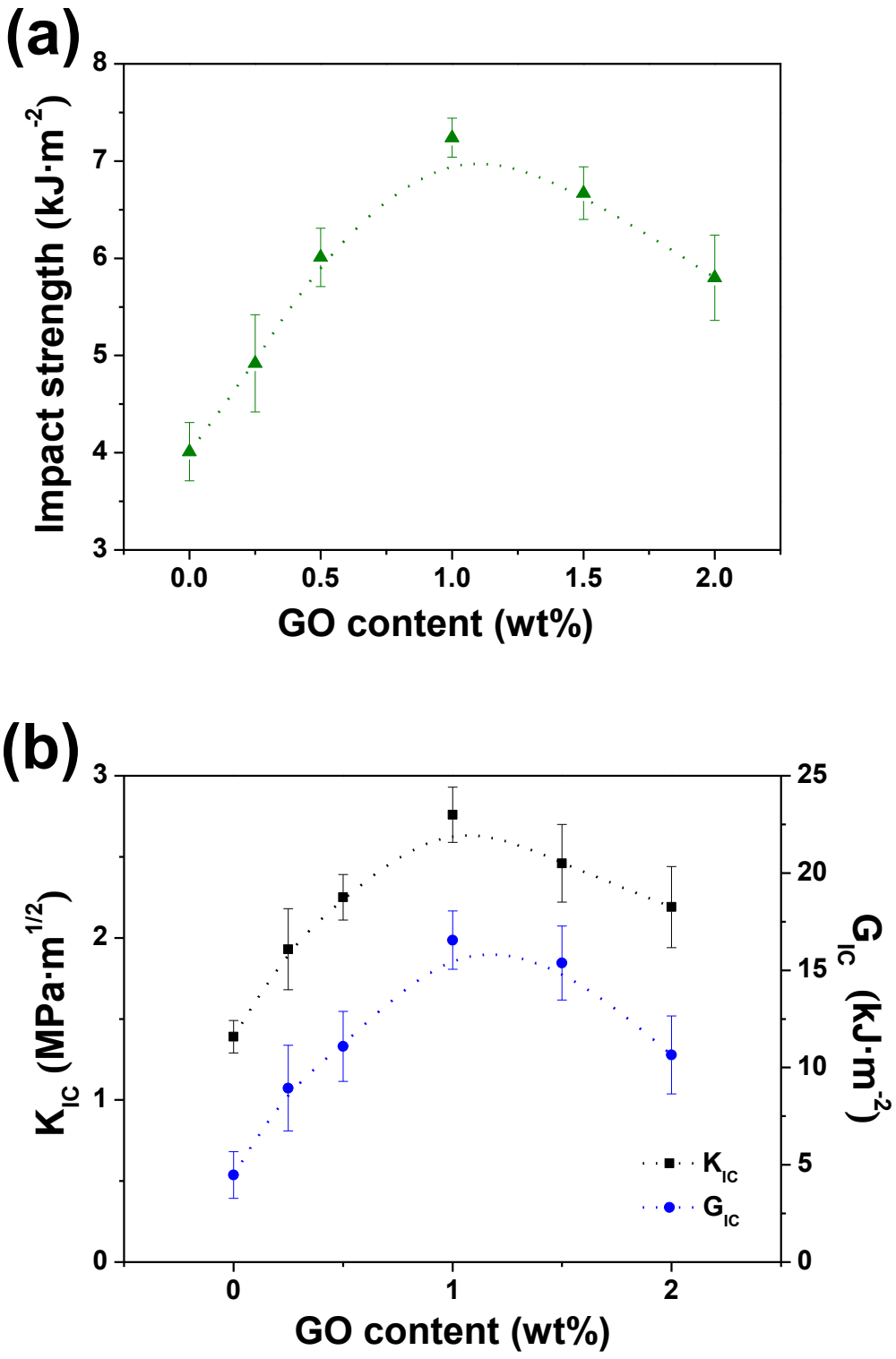

Fig. 8. Mechanical properties of GO/epoxy nanocomposites: (a) impact strength and (b) fracture toughness.

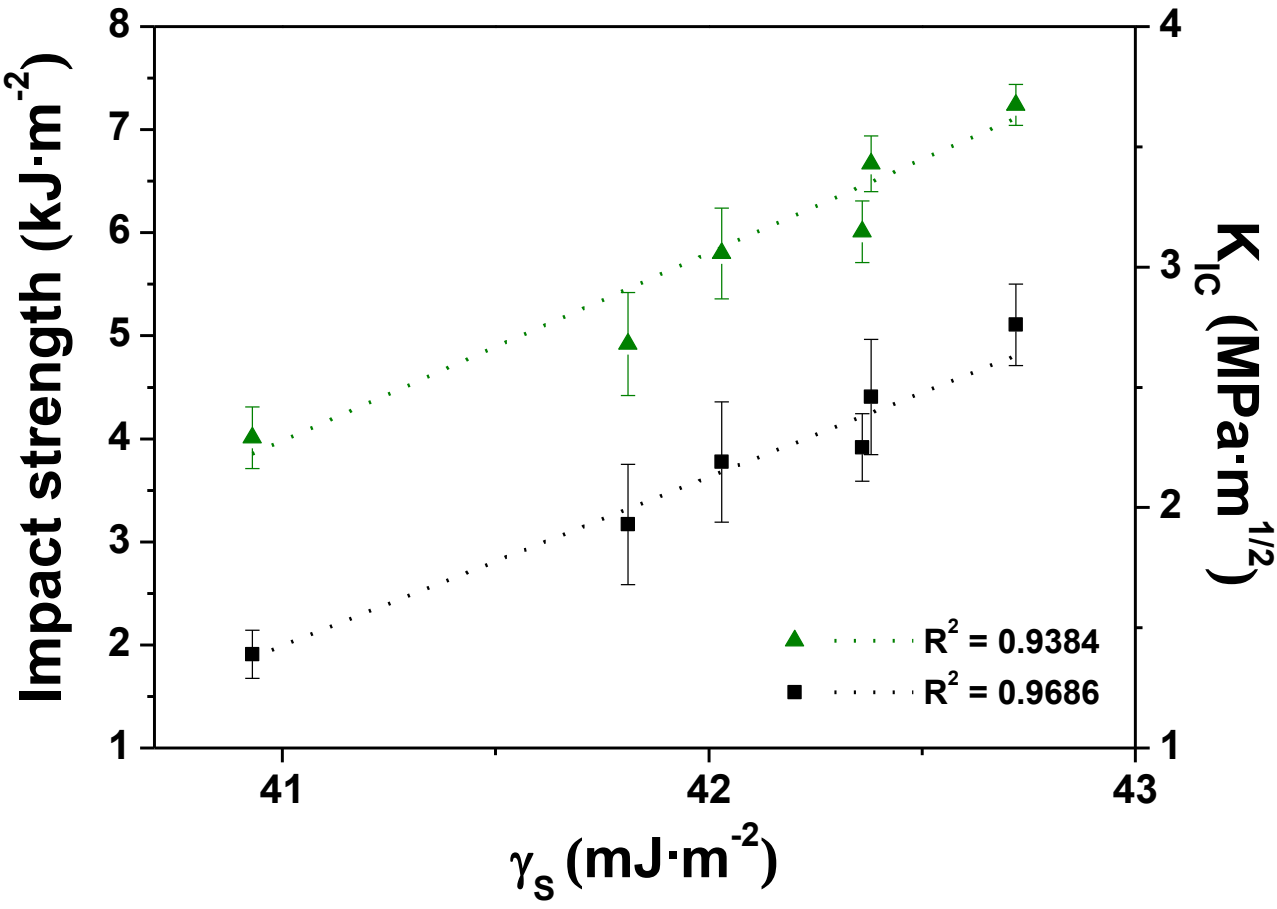

Fig. 9. Dependence of the impact strength and K_{IC} of nanocomposites on the γ_S.

Table 1 Surface tension (γ_L), London dispersive forces (γ_L^L), and specific (γ_L^{SP}) components of wetting liquids (subscript: L).

Wetting liquids	γ_L (mJ·m^{-2})	γ_L^L (mJ·m^{-2})	γ_L^{SP} (mJ·m^{-2})	γ_L^+ (mJ·m^{-2})	γ_L^- (mJ·m^{-2})
Distilled water	72.80	21.80	51.00	25.50	25.50
Diiodomethane	50.80	50.42	0.38	0.00	0.00
Ethylene glycol	47.70	31.00	16.70	1.92	47.00

Table 2 Surface free energies of GO/epoxy nanocomposites depending on GO contents.

Specimens	Surface free energy				
	γ_S (mJ·m^{-2})	γ_s^L (mJ·m^{-2})	γ_s^{SP} (mJ·m^{-2})	γ_s^+ (mJ·m^{-2})	γ_s^- (mJ·m^{-2})
Neat epoxy	40.93	39.99	0.94	9.44	0.023
0.25 wt%	41.81	40.44	1.37	17.97	0.026
0.50 wt%	42.36	40.65	1.70	22.80	0.032
1.00 wt%	42.72	40.70	2.02	27.31	0.037
1.50 wt%	42.38	40.61	1.77	24.75	0.032
2.00 wt%	42.03	40.50	1.53	24.01	0.024